







Observations on Regional Variability in Ground-Motion Amplitude from Six $M_w \sim 6.0$ Earthquakes of the North–South Seismic Zone in China

PEIBIN XU,¹  YEFEI REN,¹  RUIZHI WEN,¹  and HONGWEI WANG¹ 

Abstract—Observed ground-motion intensity for six earthquakes of $M_w = 6.0$ – 6.2 that occurred in China’s North–South Seismic Zone (NSSZ) was compared with predicted medians from the BSSA14 model. The resulting between-event (δB_e) and within-event (δW_{es}) residuals for peak ground acceleration and pseudo-spectral acceleration up to 5.0 s were used to investigate the impact of source effects and path propagation on the regional variability in observed ground-motion amplitude within the NSSZ. Although the magnitude and fault type were similar among the six earthquakes, the results showed that their source effects were significantly different, which contributed in part to the regional variability in observed ground-motion amplitude. Estimated values for stress drop were found to mirror the trend in variation of the δB_e values for short-period ground motions in the six earthquakes. This suggests that stress drop is an important factor for accurate representation of source effects and should be considered in the functional form of ground-motion prediction equations. Anelastic attenuation of ground motion was found to be considerably different in local areas of the NSSZ, which may constitute the primary reason for the regional variability in the observed ground-motion amplitude. The variation in δW_{es} values confirmed that regional adjustment of anelastic attenuation in the BSSA14 model is applicable to some local areas (i.e., around the Longmenshan fault) but not to the NSSZ in its entirety.

Key words: North–South Seismic Zone, ground motion, regional variability, source effect, anelastic attenuation.

1. Introduction

The North–South Seismic Zone (NSSZ) is widely recognized as one of the most seismically active zones in China. Based on its geological structural features and spatial seismicity characteristics, the

NSSZ (Fig. 1a) encompasses an area of approximately 2000 km (N–S) by 400 km (E–W) in western China. It extends southward from the Helan Mountains in the north of the Ningxia Hui Autonomous Region to the China–Myanmar border in Yunnan Province, crossing the western Qinling Mountains, following the track of the Longmenshan and Xianshuihe–Xiaojiang fault systems, and incorporating the Red River fault system (Ma et al. 1992; Zhang et al. 2003). The NSSZ lies between the seismically active Tibetan Plateau and the tectonically stable Ordos and South China blocks (Zhang 2013). The strong seismicity within the NSSZ results primarily from constraint arising from the Ordos and South China blocks to the continuous movement of the Tibetan Plateau northeastward in response to the northward underthrusting of the Indian Plate beneath the Eurasian Plate (Molnar and Tapponnier 1975). This complex tectonic regime has triggered many large earthquakes. For example, between 1900 and 2015, about 100 earthquakes with magnitude ≥ 6.0 have occurred in the NSSZ, as shown in Fig. 1a.

Historically, more than half of the destructive earthquakes of $M > 8.0$ in China have occurred in the NSSZ (Wang et al. 2015). In modern times, apart from the considerable number of casualties and substantial loss of property associated with several catastrophic large earthquakes (e.g., the 1920 M_L 8.6 Haiyuan earthquake and 2008 M 8.0 Wenchuan earthquakes), the frequent occurrence of and heavy damage from $M \sim 6.0$ earthquakes has been within the NSSZ. In the past decade, 10 earthquakes of $M_w = 6.0$ – 7.0 (e.g., the 2013 M_w 6.0 Minxian, 2014 M_w 6.2 Ludian, 2014 M_w 6.1 Jinggu, and 2014 M_w 6.1 Kangding earthquakes) have been measured instrumentally within the NSSZ. Considerable effort

¹ Institute of Engineering Mechanics, China Earthquake Administration, Key Laboratory of Earthquake Engineering and Engineering Vibration of China Earthquake Administration, No. 29 Xuefu Road, Harbin 150080, People’s Republic of China. E-mail: renyefei@iem.net.cn

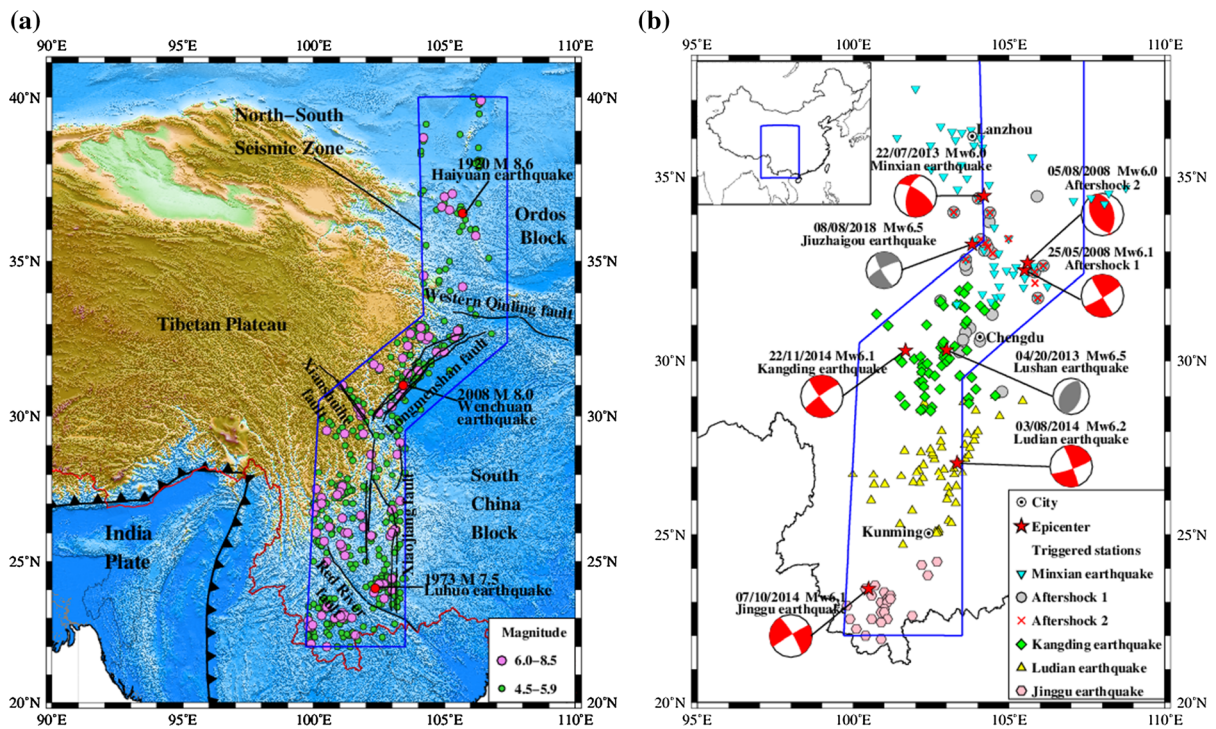


Figure 1

a Geological background in the vicinity of China's North-South Seismic Zone (NSSZ). Selected major active faults and historical earthquakes that occurred during the period from 1900 to 2015 are shown in the figure to represent the high level of seismicity. Data encompassing events with magnitude in the range of 4.5–8.5 were accessed from <http://data.earthquake.cn/>. **b** Epicenters of the Minxian, Ludian, Jinggu, and Kangding earthquakes and Wenchuan aftershocks 1 and 2 considered in this study, and triggered stations within a Joyner–Boore distance of ≤ 400 km in each event. Focal mechanisms were provided by the Global Centroid-Moment-Tensor Project (<http://www.globalcmt.org/>)

has been made by numerous earthquake engineers and seismologists in China to assess the seismic hazard of the NSSZ, and ground-motion data derived from field measurements have played an important role in many respects, such as in the development of a regional ground-motion prediction equation (GMPE). It is well known that seismic hazard analysis requires the use of GMPEs that quantify the predicted median peak ground acceleration (PGA) and response spectral parameters. The main predictive variables for GMPEs are magnitude, distance, and site. GMPEs are generally developed using regression techniques to characterize a ground-motion database that combines data from different regions. A critical assumption is that the ground-motion data from different regions in the data set are similar in terms of their embedded source and attenuation properties. The resulting equations may be biased in the median predictions for the specific site and may overestimate ground-motion

variability if there is significant regional variability in earthquake source and attenuation effects. Regional variability in any one component can manifest as ground motion variability, as has been confirmed by many previous studies (e.g., Atkinson and Morrison 2009).

As one of the key areas of national seismic monitoring and protection, strong-motion observation within the NSSZ has been greatly improved by the new generation of instruments used as part of the National Strong-Motion Observation Networks System (NSMONS) since the official commencement of the operation at the end of 2007. NSMONS has collected a large number of strong-motion recordings, especially in relation to earthquakes that have occurred within the NSSZ. In particular, numerous strong-motion recordings with considerable spatial distribution have been obtained for six $M_w \sim 6.0$ earthquakes, i.e., the 2013 M_w 6.0 Minxian

earthquake, 2014 M_w 6.2 Ludian earthquake, 2014 M_w 6.1 Jinggu earthquake, 2014 M_w 6.1 Kangding earthquake, and two aftershocks of the 2008 Wenchuan seismic sequence (M_w 6.1 event on 25 May 2008 and M_w 6.0 event on 5 August 2008), as shown in Fig. 1b. For example, 74 strong-motion recordings covering a Joyner–Boore distance (R_{JB}) of 8–327 km were collected by NSMONS during the Ludian event (Xu et al. 2015b). The occurrence of earthquakes of similar magnitude and the abundance of strong-motion recordings within the NSSZ make it a convenient area for the investigation of regional variability in ground-motion amplitude.

Various recent studies have investigated the impact of source effects (e.g., rupture directivity), propagation path (e.g., regional anelastic attenuation), and local site effects (e.g., local topography) on the ground motions observed in some moderate and large earthquakes within the NSSZ. For example, Wen and Ren (2014) investigated the hanging-wall effect on near-field ground motions, local topographic effects on recordings obtained at several stations near a fault rupture, and the effects of amplification by thick sediment on far-field ground motion in the Weihe Basin during the 2013 M_w 6.6 Lushan earthquake. By comparison with the Next Generation Attenuation (NGA) West models, Huang et al. (2013) ascribed the slower attenuation of long-period far-field ground motion during the 2013 M_w 6.0 Minxian earthquake to thick and soft loess. Rupture directivity effects on ground motions from four $M_w \sim 5.0$ aftershocks in the Lushan seismic sequence (Wen et al. 2015) and the 2014 M_w 6.1 Kangding earthquake (Wang et al. 2016) were revealed from the spatial variation in observed ground-motion intensity. Hu et al. (2016) compared the ground-motion durations of the 2014 M_w 6.2 Ludian earthquake in Yunnan Province and both the 2008 M_w 7.9 Wenchuan and the 2013 M_w 6.6 Lushan earthquakes in Sichuan Province. They found that differences in the distance dependence of ground-motion duration between the two regions were attributable to both local physical dispersion and quality factors. Ren et al. (2018) systematically compared ground-motion intensity measurements from the 2013 M_w 6.6 Lushan and the 2017 M_w 6.5 Jiuzhaigou earthquakes with predictions derived using two NGA-West2 models. They verified the

significant effects of fault type and propagation path on ground motion. These studies have generally focused on only a single earthquake or have compared the ground motion of two or three earthquakes. Thus, they have not completely revealed the regional variability in ground motion within the NSSZ.

The objective of this study was to investigate the regional variability in earthquake ground-motion amplitude observed following the occurrence of six earthquakes of $M_w = 6.0$ – 6.2 within the NSSZ (i.e., the Ludian, Jinggu, Kangding, and Minxian earthquakes and two aftershocks in the 2008 Wenchuan earthquake sequence). To pursue this objective, this work is divided into two parts. In the first part, the observed ground-motion amplitudes were compared with predicted medians from the GMPE developed by Boore et al. (2014) (hereafter, the BSSA14 model) for global shallow crustal earthquakes. Residual analysis can identify the source, site, and path that are not accounted for by GMPEs. In the second part, the between-event and within-event residuals for each earthquake were calculated and compared to investigate source and propagation path variability within the study region.

2. Earthquakes

To elucidate the differences or similarities among the characteristics of the six earthquakes, some fundamental seismic information is introduced briefly in Table 1, including earthquake date, location, magnitude, seismic intensity, and focal mechanism.

The Minxian earthquake, which was measured as M_s 6.6 by the China Earthquake Networks Center (CENC) and as M_w 6.0 by the Global Centroid-Moment-Tensor (GCMT) Project, occurred on 22 July 2013 in Minxian County in southeastern Gansu Province, with an epicenter at 34.52°N, 104.23°E and a focal depth of 20 km. This event activated the central–eastern portion of the Lintan–Dangchang thrust fault. The inverted focal mechanism and a geological field survey showed that the rupture was dominated by thrust slip and coupled with left-lateral strike slip (Zheng et al. 2013). This event caused 95 fatalities and 598 injuries [derived from the official report of the China Earthquake Administration (CEA)]. The

Table 1
Basic seismic information for the six earthquakes considered in this study

	Minxian earthquake	Ludian earthquake	Jinggu earthquake	Kangding earthquake	Wenchuan aftershock 1	Wenchuan aftershock 2
Date (local time), day/month/year	22/07/2013	03/08/2014	07/10/2014	22/11/2014	25/05/2008	05/08/2008
Latitude (°N)	104.23	103.34	100.46	101.69	105.45	105.57
Longitude (°E)	34.52	27.10	23.39	30.26	32.57	32.69
Depth (km)	20	12	5	18	14	13
M_s	6.6	6.5	6.6	6.4	6.4	6.5
M_w	6.0	6.2	6.1	6.1	6.1	6.0
Max. seismic intensity	VIII	IX	VIII	VIII	–	–
Strike/dip/rake (°)	303/66/37	71/81/– 175	329/81/174	143/85/– 1	59/84/178	348/44/103
Number of recordings ^a	52	63	24	53	24	13

The epicenter location, depth, and M_s values were provided by the China Earthquake Networks Center (CENC)

M_w , strike, dip, and slip values were provided by the Global Centroid-Moment-Tensor (GCMT) Project

^aIndicates only the number of recordings used in this study, not all those collected in each event, because only those with an R_{JB} value of < 400 km were selected

maximum macroseismic intensity in the epicentral area reached VIII on the Chinese seismic intensity scale (GB/T 17742 2008).

The Ludian earthquake, which was measured as M_s 6.5 by the CENC and as M_w 6.2 by the GCMT Project, occurred on 3 August 2014 in Ludian County in northeastern Yunnan Province, with an epicenter at 27.10°N, 103.34°E and a focal depth of 12 km. This event was a complex conjugate rupture earthquake, which simultaneously activated the NNW–SSE-trending strike-slip Zhaotong fault and the ENE–WSW-trending strike-slip Baogunao–Xiaohe fault (Zhang et al. 2014). This earthquake caused 615 fatalities, with 114 missing persons and 3143 injuries (by official report of CEA). The event caused exceptionally severe damage in the town of Longtoushan near the epicenter. The maximum macroseismic intensity reached IX on the Chinese seismic intensity scale (GB/T 17742 2008). Such serious damage with respect to such a moderate earthquake is very rare within the NSSZ. The maximum PGA recorded at station 053LLT in Longtoushan was close to 1g (where g is gravitational acceleration).

The Jinggu earthquake, which was measured as M_s 6.6 by the CENC and as M_w 6.1 by the GCMT Project, occurred on 7 October 2014 in Jinggu County in southwestern Yunnan Province, with an

epicenter at 23.39°N, 100.46°E and a shallow focal depth of 5 km. This event occurred on the extensional segment in the NNW direction of the NNW–SSE-trending strike-slip Puwen fault. It ruptured an approximately vertical fault plane (81°), striking toward the NNW (N329°), dipping toward the ENE, with a rake angle of 174°, indicating a typical strike-slip event according to the focal mechanism reported by the GCMT Project. This event caused one fatality and 323 injuries (by official report of CEA), and the maximum macroseismic intensity in the epicentral area was VIII on the Chinese seismic intensity scale (GB/T 17742 2008).

The Kangding earthquake, which was measured as M_s 6.4 by the CENC and as M_w 6.1 by the GCMT Project, occurred on 22 November 2014 in Kangding County in Sichuan Province, with an epicenter at 30.26°N, 101.69°E and a focal depth of 18 km. This event occurred on the Kangding–Daofu segment of the NNW–SSE-trending left-lateral strike-slip Xian-shuihe fault. It was characterized as a typical strike-slip mechanism with strike/dip/rake = 143°/85°/–1° reported by the GCMT Project. This event caused four fatalities and 53 injuries (by official report of CEA). The maximum macroseismic intensity in the epicentral area reached VIII on the Chinese seismic intensity scale (GB/T 17742 2008).

Two aftershocks of the 2008 Wenchuan seismic sequence were also considered in this study. One event (hereafter, WcA1), which was measured as M_s 6.4 by the CENC and as M_w 6.1 by the GCMT Project, occurred on 25 May 2008, with an epicenter at 32.57°N, 105.45°E and a focal depth of 14 km. The other event (hereafter, WcA2), which was measured as M_s 6.5 by the CENC and as M_w 6.0 by the GCMT Project, occurred on 5 August 2008, with an epicenter at 32.69°N, 105.57°E and a focal depth of 13 km. Both events occurred on the northern portion of the Longmenshan fault. WcA1 was a strike-slip event with strike/dip/rake = 149°/88°/6° reported by the GCMT Project, whereas WcA2 was a thrusting event with strike/dip/rake = 151°/47°/78° reported by the GCMT Project. As these events were aftershocks, separate information regarding numbers of casualties and seismic intensity for each event is unavailable.

Inspection of Fig. 1b reveals that the stations triggered by the six earthquakes span most of the area of the NSSZ, which confirms their suitability for use in this study to investigate the variability in the source and path propagation of ground motion. Table 1 shows that the six events have similar earthquake magnitude and impact (represented by seismic intensity) and that they are all described as shallow tectonic earthquakes. According to the focal mechanism, these events can be separated into two groups: one ascribed to strike-slip events (i.e., the Ludian, Jinggu, Kangding, and WcA1 earthquakes) and the other ascribed to thrusting events (i.e., the Minxian and WcA2 earthquakes). Thus, we consider the two groups separately in the following prediction comparison and residual analysis.

3. Overview of Strong-Motion Recordings

In this study, strong-motion data recorded at stations with R_{JB} values of < 400 km were selected because PGA and spectral ordinates at distances beyond this are too small to be of much interest to engineers. These recordings were processed uniformly using a Butterworth filter with a bandwidth of 0.1–30.0 Hz to achieve reliable estimations of PGA and spectral ordinates. The intensity measures of horizontal ground motion represented by RotD50

values (Boore 2010), including PGA and 5%-damped pseudo-spectral acceleration (PSA) at periods of 0.04–5.0 s, were calculated for these recordings. The strong-motion stations with values of R_{JB} < 400 km that recorded the six earthquakes considered are shown in Fig. 1b: 52 in the Minxian earthquake (R_{JB} = 15–395 km), 63 in the Ludian earthquake (R_{JB} = 8–327 km), 24 in the Jinggu earthquake (R_{JB} = 6–243 km), 53 in the Kangding earthquake (R_{JB} = 23–310 km), 24 in the WcA1 earthquake (R_{JB} = 27–370 km), and 13 in the WcA2 earthquake (R_{JB} = 32–253 km). Overall, 200 stations were included, and only a few stations (29) recorded more than one of the earthquakes considered. For the Minxian, Ludian, Jinggu, and Kangding earthquakes, the rupture planes for calculating the R_{JB} values were estimated according to the spatial distributions of the relocated aftershocks, as reported by Feng et al. (2013), Wang et al. (2014), Xu et al. (2015a), and Yi et al. (2015), respectively. However, this method cannot be used to estimate the rupture planes for the WcA1 and WcA2 earthquakes. Wells and Copper-smith (1994) developed empirical relationships for estimating the subsurface rupture length and the down-dip rupture width in relation to the moment magnitude. These empirical relationships were used to estimate the rupture lengths and rupture widths for the strike-slip WcA1 and reverse-slip WcA2 earthquakes, i.e., 16 × 8 km for WcA1 and 12 × 8 km for WcA2. By assuming that the original rupture occurred at the center of the rupture plane, the rupture planes for both events were constrained in the nodal planes provided by the GCMT Project mentioned above. Figure 2 shows the R_{JB} distribution of strong-motion recordings considered for the six earthquakes. Small numbers of recordings with values of R_{JB} < 50 km were obtained. Near-field strong-motion recordings with values of R_{JB} < 20 km were very limited, i.e., none were recorded in the Kangding, WcA1, or WcA2 earthquakes.

Site conditions, characterized by the time-weighted average shear-wave velocity over the upper 30 m (V_{S30}), were evaluated for all strong-motion stations considered in this study. The V_{S30} values for most stations were not measured from the velocity profile with depth $z_p \geq 30$ m. The V_{S30} values for some stations included in the NGA-West2 site database were

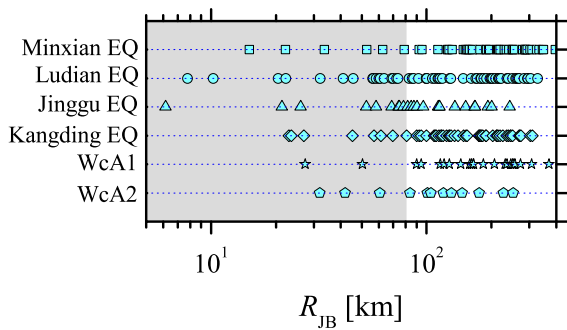


Figure 2

Joyner–Boore distance (R_{JB}) distribution for recordings considered in each of the six earthquakes selected. Shaded area indicates the range of R_{JB} (i.e., < 80 km) within which the recordings were used to calculate between-event residuals

derived from the recommended values in this database (Seyhan et al. 2014). The V_{S30} values for the remaining stations were inferred based on the empirical relationship between the site classification defined in the Code for Seismic Design of Buildings in China (GB 50011 2010) and V_{S30} , as proposed by Ren et al. (2018) for V_{S30} estimations of stations triggered in the 2017 M_s 7.0 Jiuzhaigou earthquake: Firstly, the V_{S30} values from the NGA-West2 site database for stations in western China were classified based on the site classification proposed by Lyu and Zhao (2007). The mean V_{S30} value was then calculated for the stations in each site class, which assigned values of 575.33 m/s for class I, 369.81 m/s for class II, and 236.33 m/s for class III. These values represent the approximate mean V_{S30} values for the three site classes in western China. For the stations that were not included in the NGA-West2 site database, the site classes were determined based on the method proposed by Ji et al. (2017). A flow chart was established to classify sites based on comprehensive factors of peak period, amplitude, and shape of the horizontal-to-vertical spectral ratio (HVSr) curves, which was used to determine the site classes for NSMONS stations. The HVSr was calculated using the observed recordings at these stations used in this study. The V_{S30} value for each station was then assigned by the mean of the corresponding site class.

Figure 3a shows the sources of the V_{S30} values for the strong-motion stations used in each event. It was found that V_{S30} values for most stations in the Kangding, WcA1, and WcA2 earthquakes were

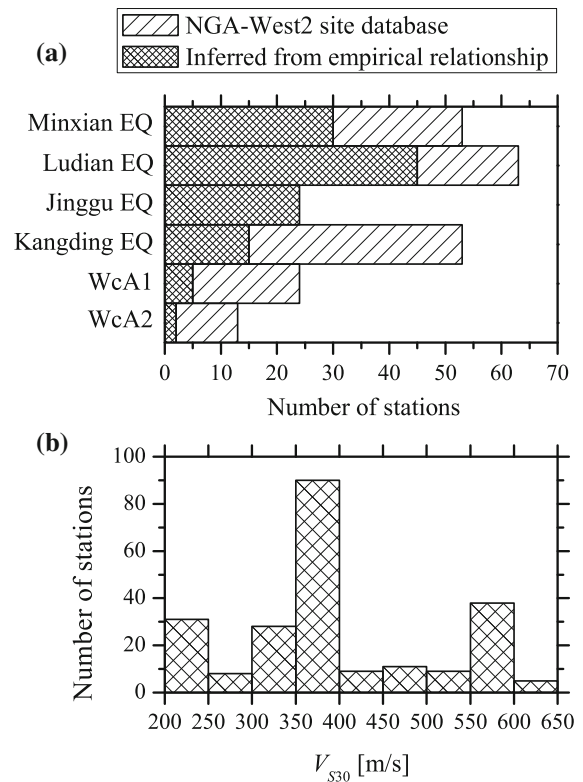


Figure 3

a Sources of V_{S30} values for strong-motion stations considered in each earthquake. **b** Histogram of V_{S30} values for all strong-motion stations considered in the six selected events

derived from the NGA-West2 site database, whereas most V_{S30} values for the Minxian and Ludian earthquakes were inferred based on empirical relationships. However, the V_{S30} values for all stations used in the Jinggu earthquake were inferred based on the empirical relationship. A histogram of the V_{S30} values for the strong-motion stations used in this study is shown in Fig. 3b. It can be seen that the V_{S30} values are largely within a range of 350–400 m/s, followed in descending order by the ranges of 550–600 and 200–250 m/s.

4. Comparisons with GMPE

Several GMPEs have been established to predict ground motion in this study region, including Lei et al. (2007), Yu and Li (2012), and Wang et al. (2013). However, some equations for the region, e.g., Lei et al. (2007) and Wang et al. (2013), were

developed only for predicting ground motion on rock sites [defined by the Code for Seismic Design of Buildings for China (GB50011 GB 50011 2010)]. Other GMPEs considered site effects with V_{S30} values that were applicable only for small to moderate earthquakes, e.g., Yu and Li (2012) for $M_s \leq 6.3$. Therefore, there is no local GMPE that is appropriate for use in this study. Five GMPEs for global shallow crustal earthquakes in active tectonic regions which were released by the NGA-West2 project have been in popular use around the world. These five GMPEs were derived by five developer teams based on the NGA-West2 database, which contains data from the Wenchuan seismic sequence in the NSSZ (Ancheta et al. 2014). One study (Ren et al. 2018) applied two NGA-West2 GMPEs (ASK14 by Abrahamson et al. 2014 and BSSA14 models) to predict ground-motion intensity measures for two moderate earthquakes (M_w 6.6 Lushan and M_w 6.5 Jiuzhaigou earthquakes) in the NSSZ. Predictions from both GMPEs represented the observations well and showed no marked discrepancies. In the current study, out of these five NGA-West2 GMPEs, we chose the BSSA14 model to provide ground-motion predictions. A combination of a base-case function and adjustments derived from analysis of residuals for the BSSA14 model are given:

$$\ln Y = F_E(M, \text{mech}) + F_P(R_{JB}, M, \text{region}) + F_S(V_{S30}, R_{JB}, M, \text{region}, z_1) + \sigma, \quad (1)$$

where $\ln Y$ is the natural logarithm of observed ground-motion intensity measures (i.e., PGA and PSA); F_E , F_P , and F_S represent functions for source, path, and site effects, respectively; σ is the total standard deviation of the model; and the predictor variables are M , mech, R_{JB} , region, V_{S30} , and z_1 . The characteristics and applied limits of these parameters are listed in Table 2. The detailed elements of F_E , F_P , and F_S are not provided, and can be found by referring to the results given by Boore et al. (2014).

The observed ground-motion amplitudes in all six events were compared with the predicted values estimated by the BSSA14 model. Observed PGA and PSA at periods of 0.5, 2.0, and 5.0 s for the four strike-slip events (i.e., the Ludian, Jinggu, Kangding, and WcA1 earthquakes) are shown in Fig. 4. The corresponding medians predicted by the BSSA14

Table 2

The key features and limits of the BSSA14 model

Parameter	Ranges
Magnitude	
M_w (strike)	[3.0, 8.5]
M_w (reverse)	[3.0, 8.5]
M_w (normal)	[3.0, 7.0]
Distance	
R_{JB}	[0, 400]
Site	
V_{S30} (m/s)	[150, 1500]
V_{S30} for reference rock (m/s)	760
Depth to V_S (km)	
$Z_{1.0}$ (km)	0–3
Regional variations	
Region	1, global; 2, China and Turkey; 3, Italy and Japan

model are also plotted in this figure. To calculate the predicted medians, the strike-slip fault type, the values of $M_w = 6.1$, $V_{S30} = 370$ m/s indicating the generic soil site, and $Z_{TOR} = 0$ km (where Z_{TOR} is the vertical depth to the shallowest point on the rupture surface), and the regional adjustment of anelastic attenuation for China were considered. Basin effects were not considered in the predicted medians. The value of $V_{S30} = 370$ m/s was derived from an average of all sites considered in this study (see Fig. 3b). It should be noted that the predicted medians do not represent real predictions at each site, as the site effects were considered uniform. The purpose of using predicted medians is to show the differences in PGA and PSA observed in different events by regarding them as benchmarks. Figure 4 shows that only the PGAs observed in WcA1 are generally larger than the predictions, while the PSAs at the 0.5-s period are close to the predictions. The PGA and PSA obtained using the BSSA14 model are over-predicted at all three periods for the other three events, even when regional adjustment for China is included. This indicates that the PGA and PSA observed at the 0.5-s period in WcA1 are generally higher than in the other three earthquakes. However, the PSAs at the 5.0-s period for WcA1 are generally smaller than in the Ludian and Jinggu earthquakes, although slightly higher than in the Kangding earthquake. These observations indicate that the variability in ground-motion amplitude is period-dependent and potentially

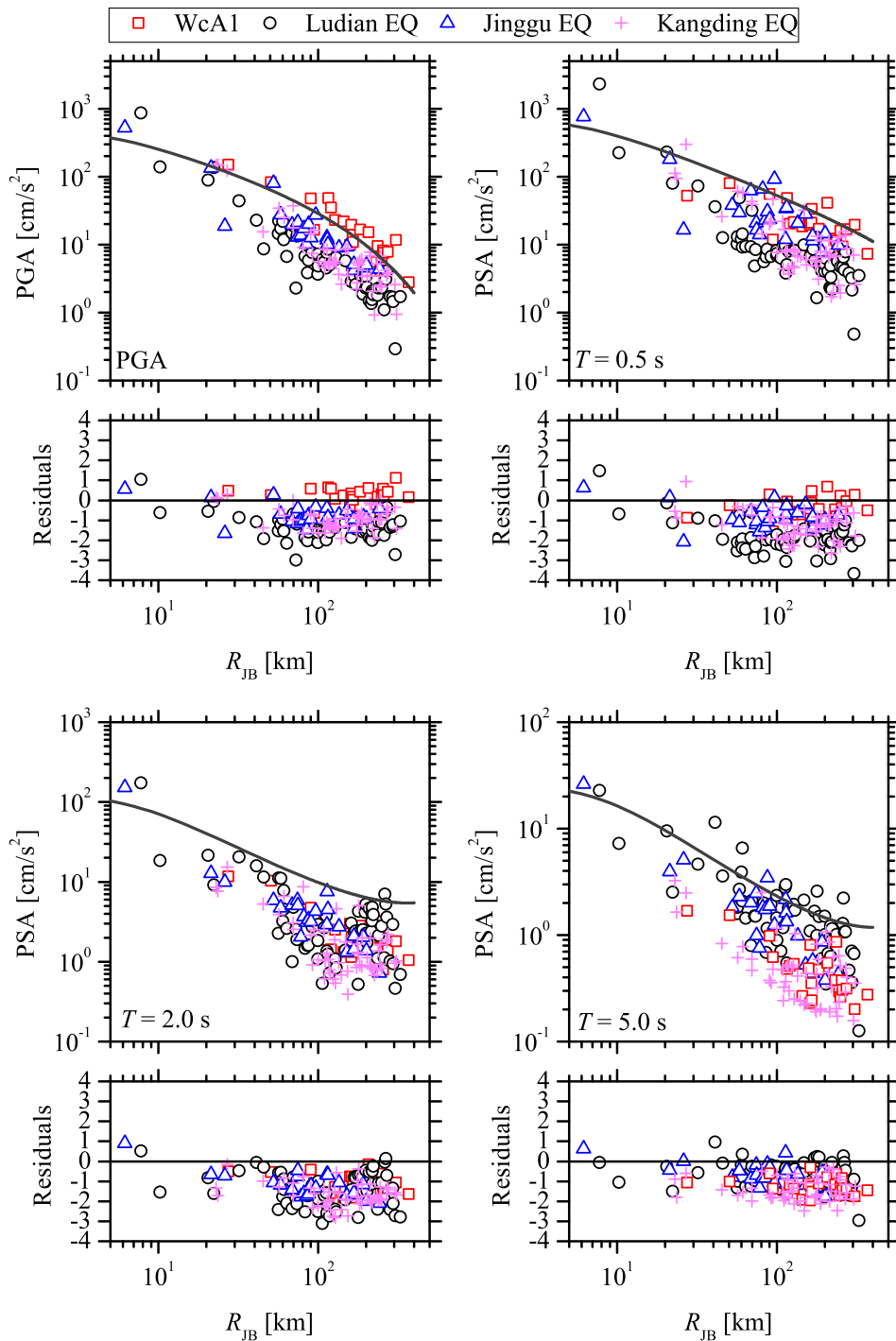


Figure 4

Observed peak ground acceleration (PGA) and 5%-damped pseudo-spectral acceleration (PSA) at periods of 0.5, 2.0, and 5.0 s for the four strike-slip events (Ludian, Jinggu, Kangding, and WcA1 earthquakes). Solid lines represent the medians predicted by the ground-motion prediction model developed by Boore et al. (2014), where strike-slip fault type, the values of $M_w = 6.1$ and $V_{S30} = 370$ m/s, and regional adjustment of anelastic attenuation for China are considered. Total residuals were calculated based on the real values of earthquake magnitude for each event and V_{S30} for each site

ascribable to the regional variability in anelastic attenuation, which is itself period-dependent.

The total residuals were calculated as the observed values minus the predicted medians on a natural logarithmic scale. A positive (negative) residual represents under-prediction (over-prediction) of the ground motion. Total residuals were calculated for the strike-slip events based on the real M_w , fault type, and $Z_{TOR} = 0$ km for each event, real V_{S30} value at each station, and regional adjustment of anelastic attenuation for China, but without consideration of the basin effects in the BSSA model, as shown in Fig. 4. The residuals of the ground-motion intensities were significantly different between the four events, highlighting the need for further investigation of the effects of regional variability in ground-motion amplitude.

The observed PGA and PSA at periods of 0.5, 2.0, and 5.0 s for the two thrusting earthquakes (i.e., the Minxian and WcA2 earthquakes) were similarly compared with the medians predicted by the BSSA14 model, as shown in Fig. 5. The reverse-slip fault type, values of $M_w = 6.0$, $V_{S30} = 370$ m/s, and $Z_{TOR} = 0$ km, and the regional adjustment of anelastic attenuation for China were considered for the calculation of the predicted medians. Basin effects were not considered in the predicted medians. The comparisons revealed that most observed values were lower than the predicted medians, as was found for the four strike-slip events, i.e., the PGA and PSA at periods of 0.5 and 5.0 s observed in both events were generally similar. However, the PSAs at the 2.0-s period observed in the far field (i.e., $R_{JB} > 100$ km) in the Minxian earthquake were generally greater than in WcA2. In particular, PSA at the 2.0-s period observed at station 061YLI in the Minxian earthquake was much greater than the predicted median. This station in the Weihe Basin is located on thick deposits (~ 700 m), and predominant site amplification at periods of 2.0–3.0 s in the standard spectral ratio of ground motions was reported by Wen and Ren (2014), which could offer a reasonable explanation for the greater PSA.

The total residuals plotted in Fig. 5 for both earthquakes were calculated based on the real values of V_{S30} for each site, as for the aforementioned four strike-slip events. Most residuals for both events are

smaller than zero, as observed for the strike-slip events in Fig. 4. The implications of this with respect to the regional variability in ground-motion amplitude are investigated in the following section using a residual analysis approach.

5. Residual Analysis

Residual analysis of strong-motion data is an effective tool with which to identify the roles of source, propagation path, and site in ground motion (Rodriguez-Marek et al. 2011; Wen et al. 2018), as these constitute the main contributors to regional variability in ground motion. The total residual (R_{es}) can be divided into the between-event residual (δB_e) and the within-event residual (δW_{es}) (Al Atik et al. 2010), i.e.,

$$R_{es} = \delta B_e + \delta W_{es}, \quad (2)$$

where subscripts “e” and “s” represent the specific earthquake and station, respectively. The terms δB_e and δW_{es} are zero-mean, independent, normally distributed random variables. The δB_e term represents the average deviation of observed ground motion associated with earthquake (e) to the median predicted by the GMPE. The δW_{es} term represents the degree of misfit between an individual observation at station (s) and the earthquake-specific (e) median prediction.

Values of R_{es} were calculated in the previous analysis, as shown in Figs. 4 and 5. For the specific earthquake, the δB_e can be obtained by the average misfit between the observed ground motion from this event and predictions based on GMPE, i.e., calculated as the mean of residuals per event. The regional adjustment of anelastic attenuation for China used in the BSSA14 model was developed based on strong-motion recordings obtained primarily from the 2008 Wenchuan earthquake sequence. For this study area, substantial differences in crustal structure among the regions of the Minxian earthquake (Gansu Province), Ludian and Jinggu earthquakes (northeastern and southwestern Yunnan Province, respectively), and Kangding earthquake (on the Xianshuihe fault in Sichuan Province) have been reported in previous studies (e.g., Wang et al. 2007; Li et al. 2012). To

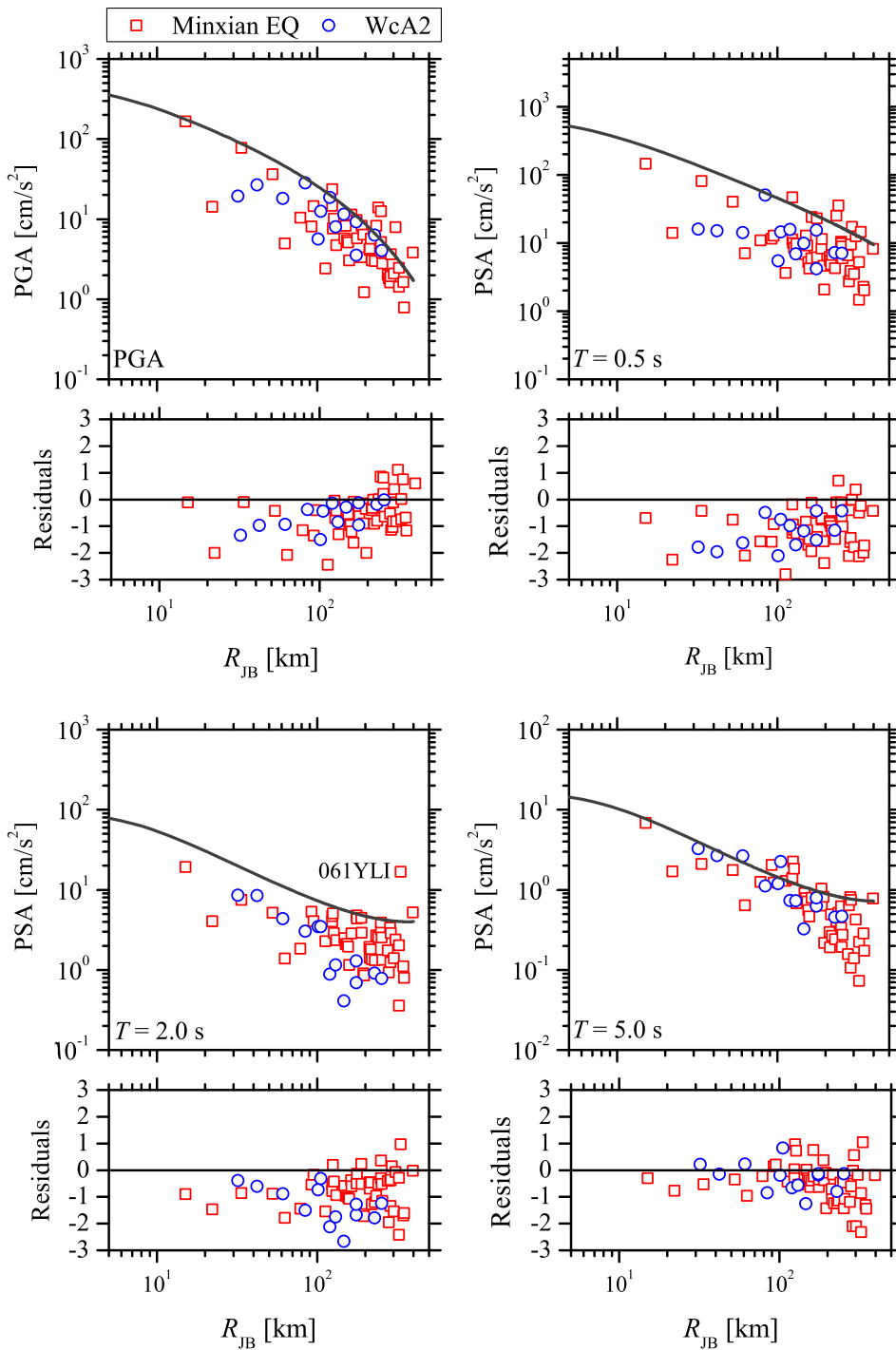


Figure 5

Observed peak ground acceleration (PGA) and 5%-damped pseudo-spectral acceleration (PSA) at periods of 0.5, 2.0, and 5.0 s for both reverse-slip events (i.e., the Minxian and WcA2 earthquakes). Solid lines represent the medians predicted by the ground-motion prediction model developed by Boore et al. (2014), where reverse-slip fault type, values of $M_w = 6.0$ and $V_{S30} = 370$ m/s, and regional adjustment of anelastic attenuation for China are considered. Total residuals were calculated based on the real values of earthquake magnitude for each event and V_{S30} for each site

ensure that δW_{es} values appropriately reveal the difference in path effects among these six events, the values of δB_e were calculated using two approaches. For WcA1 and WcA2, the adjustment was considered to be applicable because they comprised part of the 2008 Wenchuan earthquake sequence. Therefore, the δB_e values for both events were obtained by calculating the mean of the total residuals of all recordings considered. Another approach for the δB_e values involved calculations using only recordings with values of $R_{JB} < 80$ km for an individual earthquake. This was because at distances beyond 80 km, the differences in crustal structure can have a significant effect on ground motion, which can lead to variation in anelastic attenuation at large distances (e.g., quality factor) (Abrahamson et al. 2014; Boore et al. 2014). The numbers of recordings with values of $R_{JB} < 80$ km collected in these four earthquakes (i.e., Minxian, Ludian, Jinggu, and Kangding earthquakes) were adequate for calculating the values of δB_e , as shown in Fig. 2.

The δB_e values for the four strike-slip events (i.e., the Ludian, Jinggu, Kangding, and WcA1 earthquakes) are shown in Fig. 6a. For WcA1, the δB_e values are positive with respect to PGA and PSA at periods of < 0.3 s, but negative for PSA at periods of > 0.3 s. However, the δB_e values for the remaining three events are all smaller than zero for PGA and PSA at all periods up to 5.0 s. These observations indicate that the impact of source effects on ground motion for these four strike-slip events was weaker than the average for global shallow crustal earthquakes, which is considered by the BSSA14 model, with the exception of WcA1, in which the impact of source effects on short-period ground motions was stronger.

As is well known, stress drop ($\Delta\sigma$) is an important parameter closely related to high-frequency (short-period) ground-motion amplitude. With reference to a circular fault in a whole space, Eshelby (1957) obtained a value of $\Delta\sigma = 7M_0/16r^3$, where M_0 and r represent the seismic moment and the rupture radius, respectively. The value of M_0 was obtained from the M_0 - M_w relation ($M_w = (2/3) \log_{10} M_0 - 10.7$) proposed by Hanks and Kanamori (1979). The r values for the Ludian, Jinggu, and Kangding earthquakes were calculated from the rupture areas,

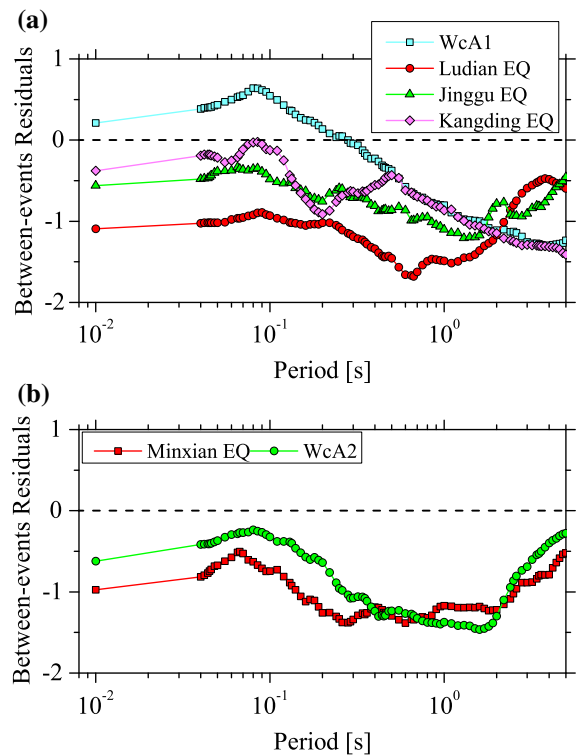


Figure 6

a Between-event residuals calculated based on the ground-motion prediction model developed by Boore et al. (2014) for four strike-slip events (i.e., the Ludian, Jinggu, Kangding, and WcA1 earthquakes). **b** Between-event residuals for two thrusting events (i.e., the Minxian and WcA2 earthquakes). Points at the 0.01-s period correspond to the between-event residuals of PGA

which were estimated from the spatial distribution of relocated aftershocks (Wang et al. 2014; Xu et al. 2015a, b; Yi et al. 2015). The areas of rupture were determined to be 568, 346, and 382 km² and the consequent $\Delta\sigma$ values were 0.92, 1.37, and 1.18 MPa for the Ludian, Jinggu, and Kangding earthquakes, respectively. However, an aftershock distribution is unavailable for WcA1 because it is itself an aftershock. Based on the values of M_0 and corner frequency (f_c) inverted using the nonparametric generalized inversion technique (Wang et al. 2018), the value of r was estimated by means of the relation between r and f_c (i.e., $r = 0.37\beta/f_c$, where $\beta = 3.6$ km/s represents the shear-wave velocity) (Brune 1970). This resulted in a value of $\Delta\sigma = 2.04$ MPa for WcA1. Variations in $\Delta\sigma$ values mirror similar variations in the δB_e values of short-period ground motions among the four events: largest for

WcA1, intermediate for the Jinggu and Kangding earthquakes, and smallest for the Ludian earthquake.

The δB_e values for the reverse-slip Minxian and WcA2 earthquakes are shown in Fig. 6b. It was found that the δB_e values for PGA and PSA at all periods up to 5.0 s were negative for both earthquakes, as established for the Jinggu, Kangding, and Ludian earthquakes. The δB_e values for PSA at periods of > 0.4 s are largely consistent in both events. However, the δB_e values for PGA and PSA at periods of < 0.4 s in the Minxian earthquake are smaller than in WcA2. According to the same method used for calculating the $\Delta\sigma$ values for the Ludian, Jinggu, and Kangding earthquakes, the value of $\Delta\sigma$ estimated for the Minxian earthquake was 0.35 MPa, slightly lower than the value of $\Delta\sigma = 0.40$ MPa for WcA2 provided by Wang et al. (2018). Differences in the $\Delta\sigma$ values between the two earthquakes may potentially explain the different δB_e values for short-period ground motions. To achieve accurate interpretation, further investigation of other factors such as source depth and slip in both space and time should be addressed.

The δB_e values between the two aftershocks of the 2008 M_w 7.9 Wenchuan earthquake (i.e., WcA1 and WcA2) are compared in Fig. 7a. It was found that the δB_e values for the strike-slip WcA1 were clearly larger than the reverse-slip WcA2 for periods < 2.5 s, whereas the opposite was observed for periods > 2.5 s. Both events had adjacent epicenter locations (see Fig. 1; Table 1), similar magnitude, and similar focal depth (i.e., $M_w = 6.1$ and 14 km for WcA1, and $M_w = 6.0$ and 13 km for WcA2). Therefore, the spectral ratios of strong-motion recordings from the same station for WcA2 and WcA1 only represent differences in source effects. Figure 7b shows the Fourier amplitude spectral ratios of WcA2 to WcA1 calculated using strong-motion recordings at 12 stations triggered in both events. The trend in spectral ratios versus period is largely consistent with that shown by the δB_e values between the two events. However, this finding is contrary to some previous studies (e.g., Bommer et al. 2003; Ren et al. 2018), which have reported that a reverse-slip earthquake might generally be expected to produce ground motions with greater (lower) amplitude at short and intermediate (long) periods than a strike-slip event. As mentioned above, the value of stress drop is

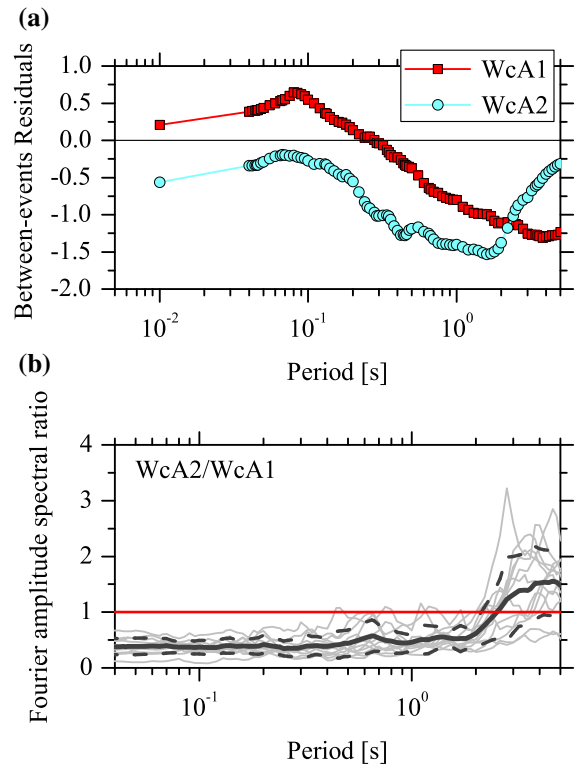


Figure 7

a Comparison of between-event residuals in two aftershocks of the M_w 7.9 Wenchuan earthquake: WcA1 and WcA2. Points at the 0.01-s period correspond to the between-event residuals of PGA. **b** Observed Fourier amplitude spectral ratios of WcA2 to WcA1 using strong-motion recordings obtained at 12 stations triggered in both events. Black solid line represents the mean value of the 12 individual spectral ratios (gray solid lines), and the dashed lines represent the mean \pm one standard deviation

considerably different between the two events (i.e., 2.04 MPa for WcA1 and 0.40 MPa for WcA2), which might have a much more important influence than fault type on source effects. Bindi et al. (2017) used seismological models extracted from S-wave spectra recorded in central Italy to interpret the between-event variability computed for local GMPEs. The results showed that δB_e was clearly dependent on stress drop for frequencies > 2.0 Hz; thus, the introduction of an empirical $\Delta\sigma$ estimate as an explanatory variable in the GMPE could strongly reduce the between-event variability. Our observations shown in Figs. 6 and 7 might support their conclusion and thus could facilitate an improvement in the functional form of GMPEs by considering

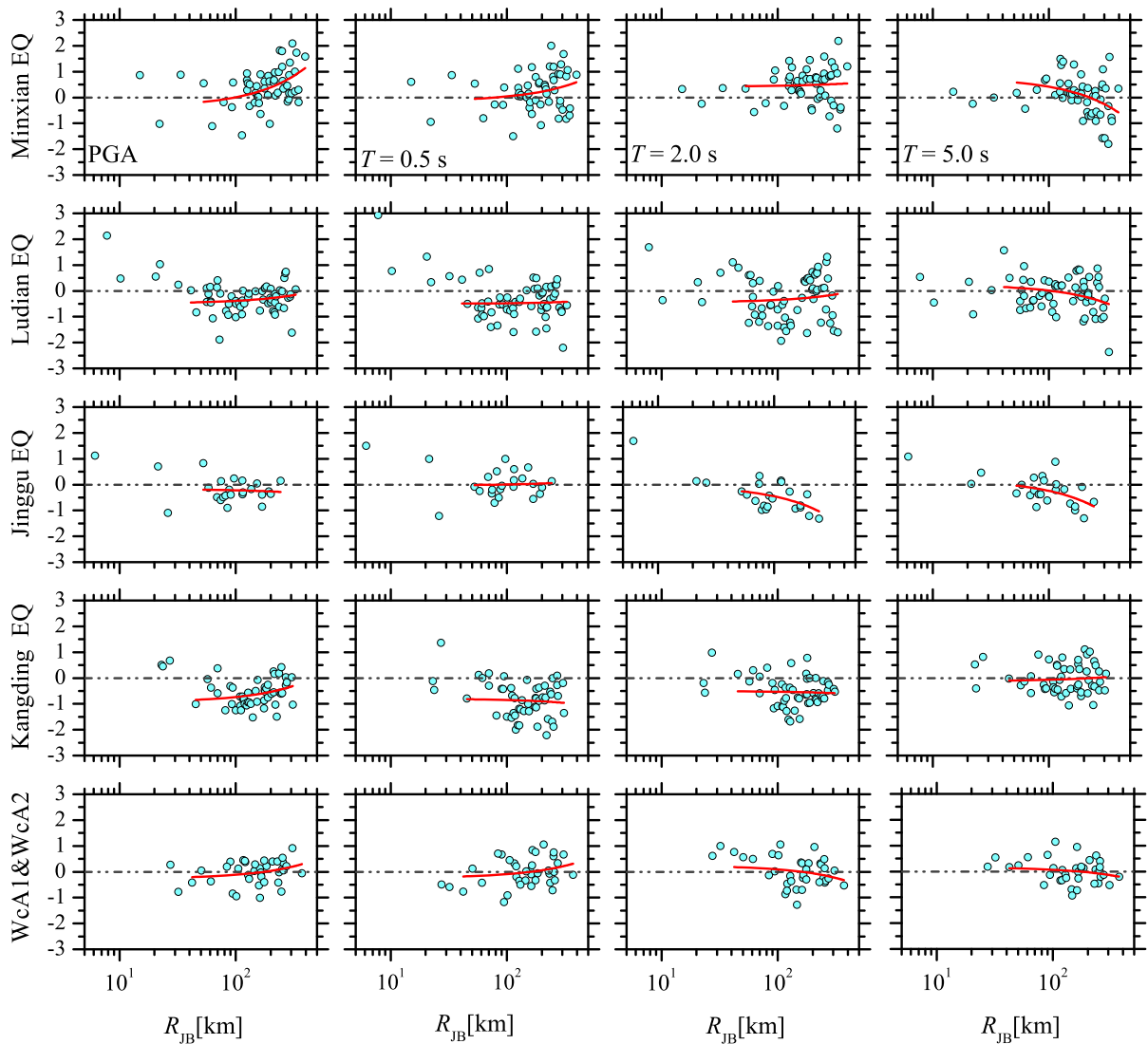


Figure 8

Within-event residuals for PGA and PSA at periods of 0.5, 2.0, and 5.0 s versus R_{JB} . Trend lines for δW_{es} versus R_{JB} were regressed linearly for each earthquake based on data in the range $R_{JB} = 40\text{--}400$ km

stress drop as an important factor representing source effects.

The δW_{es} values for PGA and PSA at periods of 0.04–5.0 s were calculated according to Eq. (2). Figure 8 shows the within-event residuals versus R_{JB} for PGA and PSA at $T = 0.5, 2.0,$ and 5.0 s for each event. Because only 13 strong-motion recordings obtained in WcA2 (see Table 1) were used in this study, the number of recordings is considered inadequate to evaluate path effects. We combined the data

from WcA1 and WcA2 and considered that their δW_{es} values represented the path effects of the same local area because of their close epicentral locations (see Fig. 1). Clear trends of increasing and decreasing δW_{es} versus R_{JB} are visible, and the patterns vary markedly between different ground-motion intensities and different events. For the Minxian earthquake, a clearly upward trend is observed for PGA and PSA at period $T = 0.5$ s, but a flat trend is evident for PSA at period $T = 2.0$ s, and a downward trend is found

for PSA at period $T = 5.0$ s. For the Ludian earthquake, flat trends are observed for PGA and PSA at periods $T = 0.5$ and 2.0 s, but a decreasing trend is evident for PSA at period $T = 5.0$ s. For the Jinggu earthquake, flat trends are observed for PGA and PSA at period $T = 0.5$ s, and a clearly decreasing trend is evident for PSA at periods $T = 2.0$ and 5.0 s. For the Kangding earthquake, a slightly increasing trend is observed for PGA, but flat trends are evident for PSA at periods $T = 0.5, 2.0,$ and 5.0 s. For both Wenchuan aftershocks, a slightly upward trend is observed for both PGA and PSA at period $T = 0.5$ s, and a slightly downward trend is observed for PSA at periods $T = 2.0$ and 5.0 s. These findings indicate strong regional variability and period dependence of anelastic attenuation in the NSSZ, associated with the variability in regional tectonic setting and the heterogeneity of the crustal structure.

To investigate the trend for δW_{es} versus R_{JB} for PSA at additional periods, we fitted a linear expression between the values of δW_{es} and R_{JB} following the study by Boore et al. (2014):

$$\delta W_{es} = \Delta c_3(R_{JB} - R_{ref}) + \delta W_R, \quad (3)$$

where Δc_3 is an adjustment coefficient of anelastic attenuation, δW_R is the approximate mean of the δW_{es} values at close distances, and the reference distance R_{ref} is fixed at 1.0 km. The term Δc_3 can be considered a quantitative representation of the anelastic attenuation, i.e., a positive (negative) Δc_3 value indicates weak (strong) anelastic attenuation.

To ensure a reliable regression, we limited the data to the range with $R_{JB} > 40$ km because there were too few data with $R_{JB} < 40$ km. The Δc_3 values for PSA at periods ranging from 0.04 to 5.0 s are shown in Fig. 9. The values of Δc_3 are significantly different between earthquakes, indicating different anelastic attenuation of ground-motion amplitude within local areas of the NSSZ. This shows that anelastic attenuation for short-period ground motion (i.e., < 0.3 s) is weakest (strongest) around the Minxian (Jinggu) area. The anelastic attenuation for long-period ground motion (i.e., > 2.0 s) is strongest around the Kangding area. The variation in Δc_3 values with period is much larger for the Minxian, Ludian, Jinggu, and Kangding earthquakes than for the WcA1 and WcA2 earthquakes, for which the

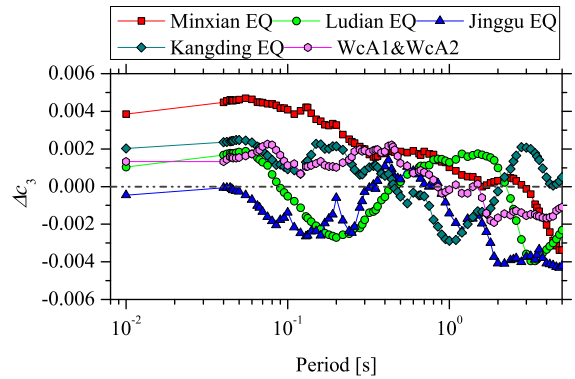


Figure 9

The Δc_3 values derived from the linear regression between within-event residuals and R_{JB} for PGA and PSA at periods of 0.04 – 5.0 s. Points at the 0.01 -s period correspond to Δc_3 values for PGA

variation in Δc_3 values with period is small (within ± 0.002). This might be attributable to the use of the regional adjustment of anelastic attenuation in the BSSA14 model, which was developed based predominantly on strong-motion data from the 2008 Wenchuan aftershocks.

To investigate the applicability of the regional adjustment of anelastic attenuation in the BSSA14 model to the NSSZ, the Δc_3 values were computed again using all the data from the six earthquakes considered, as shown in Fig. 10. The within-event residuals for all data versus R_{JB} for PGA and PSA at periods of $0.5, 2.0,$ and 5.0 s are plotted in Fig. 10a. Increasing and decreasing trends in δW_{es} versus R_{JB} are visible for all four ground-motion intensities, similar to Fig. 8. Figure 10b shows that the values of Δc_3 are not close to zero at most periods, although the regional adjustment of anelastic attenuation in the BSSA14 model was considered in this study. The Δc_3 values are all positive (negative) at periods of < 2.5 s (> 2.5 s), implying a difference in the average anelastic attenuation between the NSSZ and the region (mainly around the Longmenshan fault) considered in the BSSA14 model.

We compared the Δc_3 values in this study with those for the Lushan and Jiuzhaigou earthquakes provided by Ren et al. (2018), which were also calculated based on the BSSA14 model. It should be noted that both the Lushan and the Jiuzhaigou earthquakes also occurred within the NSSZ (see

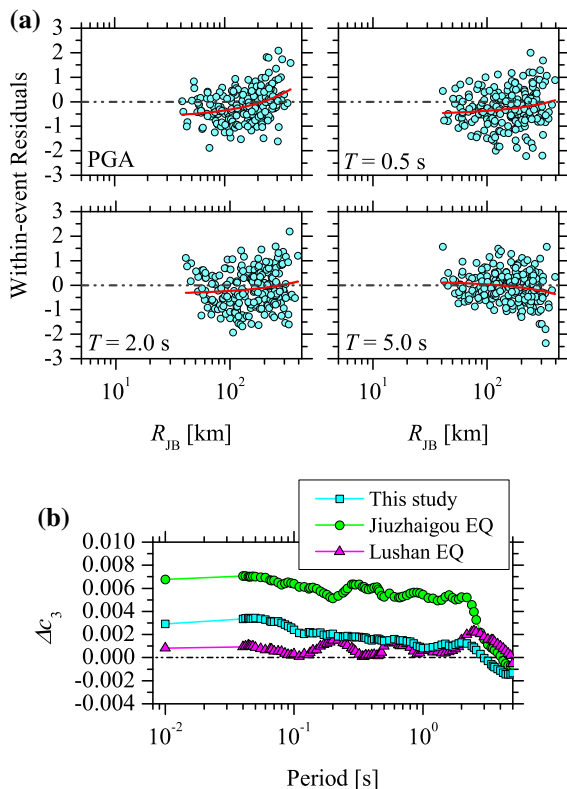


Figure 10

a Within-event residuals for PGA and PSA at periods of 0.5, 2.0, and 5.0 s versus R_{JB} . Trend lines for δW_{es} versus R_{JB} were regressed linearly based on data in the range $R_{JB} = 40\text{--}400$ km. **b** Comparison of Δc_3 values from the six earthquakes considered in this study with those from the Jiuzhaigou and Lushan earthquakes given by Ren et al. (2018). Points at the 0.01-s period correspond to Δc_3 values for PGA

Fig. 1b). The Δc_3 values for the Lushan earthquake are close to zero at most periods, as shown in Fig. 9 for WcA1 and WcA2. These earthquakes all occurred on the Longmenshan fault, validating the applicability of the regional adjustment of anelastic attenuation in the BSSA14 model to this local area. The Δc_3 values for the Jiuzhaigou earthquake deviate markedly from zero at $T < 2.5$ s, and they are much larger than derived for the six earthquakes considered in this study. This finding indicates that the regional adjustment of anelastic attenuation in the BSSA14 model might not be applicable to a wider region, such as the NSSZ. Additional strong-motion data from earthquakes in other areas of China will be needed to develop other regional adjustments for the BSSA14 model.

6. Conclusions

This study investigated the regional variability in ground-motion amplitude revealed in six $M_w \sim 6.0$ earthquakes that occurred within China's NSSZ: the 2013 M_w 6.0 Minxian earthquake, 2014 M_w 6.2 Ludian earthquake, 2014 M_w 6.1 Jinggu earthquake, 2014 M_w 6.1 Kangding earthquake, and two aftershocks (referred to as WcA1 and WcA2 in this study) of the 2008 M_w 7.9 Wenchuan earthquake. Strong-motion recordings collected in these earthquakes were used, and the observed PGA and PSA were compared with the predicted medians provided by the BSSA14 model. Their between-event residuals (δB_e) and within-event residuals (δW_{es}) were analyzed to interpret the implications regarding the impact of source effects and path propagation on the regional variability in observed ground-motion amplitude. A number of major conclusions were drawn based on this analysis.

1. Generally, the PGA and PSA at periods of 0.5, 2.0, and 5.0 s observed in the six earthquakes were smaller than the predicted medians from the BSSA14 model, with the exception of the PGA observed in WcA1. The observed ground-motion amplitude varied markedly among the six earthquakes considered.
2. The δB_e values were positive with respect to PGA and PSA at periods of < 0.3 s for WcA1, whereas they were all smaller than zero for all PSAs at periods of up to 5.0 s for the other five events. This indicates that the impact of source effects on ground motion for all events is weaker than the average level for global shallow crustal earthquakes considered by the BSSA14 model, except for WcA1, in which a stronger impact of source effects on short-period ground motion was observed. The estimated $\Delta\sigma$ values showed variations among the six earthquakes that mirrored the trend in variation of δB_e values for short-period ground motions, suggesting the need for additional consideration of stress drop in the functional form of GMPEs to accurately represent source effects.
3. The Δc_3 values were obtained via linear regression of the δW_{es} values versus R_{JB} to quantitatively represent the anelastic attenuation of ground

motions within the NSSZ. The results showed that Δc_3 values differed markedly among the six earthquakes studied. This finding indicates that different anelastic attenuation in local areas of the NSSZ might represent the major cause of the observed regional variability in ground-motion amplitude. The Δc_3 values derived from the data for all the earthquakes verified that regional adjustment of anelastic attenuation in the BSSA14 model is applicable to some local areas (i.e., around the Longmenshan fault) but not to the NSSZ in its entirety.

Acknowledgements

The fatality and injury numbers and the macroseismic intensity map were obtained from the official website of the China Earthquake Administration <http://www.cea.gov.cn> (last accessed February 2018), in Chinese. Strong-motion recordings were collected by the China Strong-Motion Network Center. Due to the current maintenance of the website (<http://www.csmnc.net/>) (official notice of Institute of Engineering Mechanics, CEA can be obtained at <http://www.iem.ac.cn/detail.html?id=1102>), we contacted the email csmnc@iem.ac.cn for data application (last accessed June 2017). Basic information on earthquakes, including surface wave magnitude and hypocentral location was derived from the China Earthquake Network Center website at <http://news.ceic.ac.cn/> (last accessed June 2017). The moment magnitudes and focal mechanisms in the Centroid-Moment-Tensor catalog were obtained from the Global CMT website at <http://www.globalcmt.org/> (last accessed December 2017). The V_{S30} values for some stations were obtained from the Next Generation Attenuation (NGA) program database of the Pacific Earthquake Engineering Research Center, available at <http://peer.berkeley.edu/nga/> (last accessed August, 2017). Some of the plots were produced using Generic Mapping Tools (Wessel and Smith 1991). This study was supported by the National Key R&D Program of China (no. 2017YFC1500801), National Natural Science Foundation of China (nos. 51878632 and 51808514), and Science Foundation of

the Institute of Engineering Mechanics, CEA (no. 2016A04). The authors are grateful to two anonymous revisers for their valuable comments and suggestions, which helped improve the manuscript.

Open Access This article is distributed under the terms of the Creative Commons Attribution 4.0 International License (<http://creativecommons.org/licenses/by/4.0/>), which permits unrestricted use, distribution, and reproduction in any medium, provided you give appropriate credit to the original author(s) and the source, provide a link to the Creative Commons license, and indicate if changes were made.

Publisher's Note Springer Nature remains neutral with regard to jurisdictional claims in published maps and institutional affiliations.

REFERENCES

- Abrahamson, N. A., Silva, W. J., & Kamai, R. (2014). Summary of the Ask14 ground motion relation for active crustal region. *Earthquake Spectra*, 30(3), 1025–1055. <https://doi.org/10.1193/070913eqs198m>.
- Al Atik, L., Abrahamson, N. A., Bommer, J. J., Scherbaum, F., Cotton, F., & Kuehn, N. (2010). The variability of ground-motion prediction models and its components. *Seismological Research Letters*, 81(5), 794–801. <https://doi.org/10.1785/gssrl.81.5.794>.
- Ancheta, T. D., Darragh, R. B., Stewart, J. P., Seyhan, E., Silva, W. J., Chiou, B. S.-J., et al. (2014). NGA-West2 database. *Earthquake Spectra*, 30, 989–1005. <https://doi.org/10.1193/070913EQS197M>.
- Atkinson, G. M., & Morrison, M. (2009). Observations on regional variability in ground-motion amplitudes for small-to-moderate earthquakes in North America. *Bulletin of the Seismological Society of America*, 99(4), 2393–2409. <https://doi.org/10.1785/0120080223>.
- Bindi, D., Spallarossa, D., & Pacor, F. (2017). Between-event and between-station variability observed in the Fourier and response spectra domains: Comparison with seismological models. *Geophysical Journal International*, 210(2), 1092–1104. <https://doi.org/10.1093/gji/ggx217>.
- Bommer, J. J., Douglas, J., & Strasser, F. O. (2003). Style-of-faulting in ground-motion prediction equations. *Bulletin of Earthquake Engineering*, 1(2), 171–203. <https://doi.org/10.1023/A:1026323123154>.
- Boore, D. M. (2010). Orientation-independent, non geometric-mean measures of seismic intensity from two horizontal components of motion. *Bulletin of the Seismological Society of America*, 100(4), 1830–1835. <https://doi.org/10.1785/0120090400>.
- Boore, D. M., Stewart, J. P., Seyhan, E., & Atkinson, G. M. (2014). NGA-West2 equations for predicting PGA, PGV, and 5% damped PSA for shallow crustal earthquakes. *Earthquake*

- Spectra*, 30(3), 1057–1085. <https://doi.org/10.1193/070113EQS184M>.
- Brune, J. (1970). Tectonic stress and the spectra of seismic shear waves from earthquakes. *Journal of Geophysical Research*, 75(26), 4997–5009. <https://doi.org/10.1029/JB075i026p04997>.
- Eshelby, J. D. (1957). The determination of the elastic field of an ellipsoidal inclusion, and related problems. *Proceedings of the Royal Society*, 241(1226), 376–396. <https://doi.org/10.1098/rspa.1957.0133>.
- Feng, Y. W., Zhang, Y. S., Liu, X. Z., Chen, J. F., Yao, H. D., & Zhang, X. (2013). Relocation of mainshock and aftershocks of the 2013 Minxin-Zhangxian M_s 6.6 earthquake in Gansu. *China Earthquake Engineering Journal*, 35(3), 443–447. <https://doi.org/10.3969/j.issn.1000-0844.2013.0443>. (in Chinese).
- GB 50011. (2010). *Code for seismic design of buildings*. Beijing: China Architecture Industry Press. (in Chinese).
- GB/T 17742. (2008). *The Chinese Seismic Intensity Scale*. Beijing: Standard Press of China. (in Chinese).
- Hanks, T. C., & Kanamori, H. (1979). A moment magnitude scale. *Journal of Geophysical Research*, 84(B5), 2348–2350. <https://doi.org/10.1029/JB084iB05p02348>.
- Hu, J. J., Zhang, Q., Jiang, Z. J., Xie, L. L., & Zhou, B. F. (2016). Characteristics of strong ground motions in the 2014 M_s 6.5 Ludian earthquake, Yunnan. *China Journal of Seismology*, 20(1), 361–373. <https://doi.org/10.1007/s10950-015-9532-x>.
- Huang, X. T., Wen, R. Z., Ren, Y. F., & Xu, P. B. (2013). Strong motion records and its characteristics in Minxian-Zhangxian M_s 6.6 earthquake on July 22, 2013. *China Earthquake Engineering Journal*, 35(3), 489–496. <https://doi.org/10.3969/j.issn.1000-0844.2013.03.0489>. (in Chinese).
- Ji, K., Ren, Y. F., & Wen, R. Z. (2017). Site classification for National Strong Motion Observation Network System (NSMONS) stations in China using an empirical H/V spectral ratio method. *Journal of Asian Earth Sciences*, 147, 79–94. <https://doi.org/10.1016/j.jseae.2017.07.032>.
- Lei, J. C., Gao, M. T., & Yu, Y. X. (2007). Seismic motion attenuation relations in Sichuan and adjacent areas. *Acta Seismologica Sinica*, 29, 500–511. <https://doi.org/10.1007/s11589-007-0532-y>. (in Chinese).
- Li, Z. W., Ni, S. D., Hao, T. Y., Hu, Y., & Roecker, S. (2012). Uppermost mantle structure of the eastern margin of the Tibetan plateau from interstation Pn traveltimes difference tomography. *Earth and Planetary Science Letters*, 335(336), 195–205. <https://doi.org/10.1016/j.epsl.2012.05.005>.
- Lyu, H. S., & Zhao, F. X. (2007). Site coefficients suitable to China site category. *Acta Seismologica Sinica*, 20, 71–79. <https://doi.org/10.1007/s11589-007-0071-6>. (in Chinese).
- Ma, Z. J., Li, X. Z., & Jin, J. Y. (1992). The law interpretation and prediction of earthquake migration-earthquake migration of four seismic belts in China mainland. *Seismology and Geology*, 14(2), 129–139. (in Chinese).
- Molnar, P., & Tapponnier, P. (1975). Cenozoic tectonics of Asia: Effects of a continental collision: Features of recent continental tectonics in Asia can be interpreted as results of the India-Eurasia collision. *Science*, 189, 419–426. <https://doi.org/10.1126/science.189.4201.419>.
- Ren, Y. F., Wang, H. W., Xu, P. B., Dhakal, Y. P., Wen, R. Z., Ma, Q., et al. (2018). Strong-motion observations of the 2017 M_s 7.0 Jiuzhaigou earthquake: Comparison with the 2013 M_s 7.0 Lushan earthquake. *Seismological Research Letters*, 89(4), 1354–1365. <https://doi.org/10.1785/0220170238>.
- Rodriguez-Marek, A., Montalva, G. A., Cotton, F., & Bonilla, F. (2011). Analysis of single-station standard deviation using the KiK-net data. *Bulletin of the Seismological Society of America*, 101(3), 1242–1258. <https://doi.org/10.1785/0120100252>.
- Seyhan, E., Stewart, J. P., Ancheta, T. D., Darragh, R. B., & Graves, R. W. (2014). NGA-West2 site database. *Earthquake spectra*, 30(3), 1007–1024. <https://doi.org/10.1193/062913EQS180M>.
- Wang, C. Y., Han, W. B., Wu, J. P., Luo, H., & Chan, W. W. (2007). Crustal structure beneath the eastern margin of the Tibetan plateau and its tectonics implications. *Journal of Geophysical Research Solid Earth*, 112, B07307. <https://doi.org/10.1029/2005JB003873>.
- Wang, Y. S., Li, X. J., & Zhou, Z. H. (2013). Research on attenuation relationships for horizontal strong ground motions in Sichuan-Yunnan region. *Acta Seismologica Sinica*, 35, 238–239. <https://doi.org/10.3969/j.issn.0253-3782.2013.02.010>. (in Chinese).
- Wang, X. S., Lv, J., Xie, Z. J., Long, F., Zhan, X. Y., & Zheng, Y. (2015). Focal mechanisms and tectonic stress field in the North-South Seismic Belt of china. *Chinese Journal of Geophysics*, 58(11), 4149–4162. <https://doi.org/10.6038/cjg20151122>. (in Chinese).
- Wang, H., Ren, Y., & Wen, R. (2018). Source parameters, path attenuation and site effects from strong-motion recordings of the Wenchuan aftershocks (2008–2013) using a non-parametric generalized inversion technique. *Geophysical Journal International*, 212, 872–890. <https://doi.org/10.1093/gji/ggx447>.
- Wang, H. W., Wen, R. Z., Ren, Y. F., & Song, J. D. (2016). Rapid rupture direction estimation of Kangding earthquake using strong-motion recordings. *Journal of Southwest Jiaotong University*, 51(6), 1138–1146. <https://doi.org/10.3969/j.issn.0258-2724.2016.06.013>. (in Chinese).
- Wang, W. L., Wu, J. P., Fang, L. H., & Lai, G. J. (2014). Double difference location of the Ludian M_s 6.5 earthquake sequences in Yunnan province in 2014. *Chinese Journal of Geophysics*, 57(9), 3042–3051. <https://doi.org/10.6083/cjg20140929>. (in Chinese).
- Wells, D. L., & Coppersmith, K. J. (1994). New empirical relationships among magnitude, rupture length, rupture width, rupture area, and surface displacement. *Bulletin of the Seismological Society of America*, 84(4), 974–1002.
- Wen, R. Z., & Ren, Y. F. (2014). Strong-motion observations of the Lushan earthquake on 20 April 2013. *Seismological Research Letters*, 85(5), 1043–1055. <https://doi.org/10.1785/0220140006>.
- Wen, R. Z., Wang, H. W., & Ren, Y. F. (2015). Rupture directivity from strong-motion recordings of the 2013 Lushan aftershocks. *Bulletin of the Seismological Society of America*, 105(6), 3068–3082. <https://doi.org/10.1785/0120150100>.
- Wen, R. Z., Xu, P. B., Wang, H. W., & Ren, Y. F. (2018). Single-station standard deviation using strong-motion data from Sichuan Region, China. *Bulletin of the Seismological Society of America*, 108(4), 2237–2247. <https://doi.org/10.1785/0120170276>.
- Wessel, P., & Smith, W. H. F. (1991). Free software helps map and display data. *Eos Transactions AGU*, 72, 441.
- Xu, F. K., Liu, Z. F., Zhang, Z. Q., Li, J., Liu, L. F., & Su, Y. J. (2015a). Double difference relocation and focal mechanisms of the Jingu M_s 6.6 earthquake sequences in Yunnan Province in 2014. *Earth Science-Journal of China University of Geosciences*, 40(10), 1741–1754. <https://doi.org/10.3799/dqkx.2015.156>. (in Chinese).

- Xu, P. B., Wen, R. Z., Wang, H. W., Ji, K., & Ren, Y. F. (2015b). Characteristics of strong motions and damage implications of M_s 6.5 Ludian earthquake on August 3, 2014. *Earthquake Science*, 28(1), 17–24. <https://doi.org/10.1007/s11589-014-0104-x>.
- Yi, G. X., Long, F., Wen, X. Z., Liang, M. J., & Wang, S. W. (2015). Seismogenic structure of the M 6.3 Kangding earthquake sequence on 22 Nov 2014, Southwestern China. *Chinese Journal of Geophysics*, 58(4), 1205–1219. <https://doi.org/10.6038/cjg20150410>. (in Chinese).
- Yu, T., & Li, X. J. (2012). Attenuation relationship of ground motion for Wenchuan earthquake region based on NGA model. *Chinese Journal of Geotechnical Engineering*, 34, 552–558. (in Chinese).
- Zhang, P. Z. (2013). A review on active tectonics and deep crustal processes of the Western Sichuan region, eastern margin of the Tibetan Plateau. *Tectonophysics*, 584(1), 7–22. <https://doi.org/10.1016/j.tecto.2012.02.021>.
- Zhang, G. W., Lei, J. S., Liang, S. S., & Sun, C. Q. (2014). Relocations focal mechanism solutions of the 3 August 2014 Ludian, Yunnan M_s 6.5 earthquake sequence. *Chinese Journal of Geophysics*, 57(9), 3018–3027. <https://doi.org/10.6083/cjg20140926>. (in Chinese).
- Zhang, J. S., Li, Y., & Han, Z. J. (2003). Deformation responses to eastwards escaping of the Qinghai-Tibet plateau and tectonics of the south-north seismic zones in China. *Earth Science Frontiers*, 10(u08), 168–175. <https://doi.org/10.3321/j.issn:1005-2321.2003.z1.024>. (in Chinese).
- Zheng, W. J., Yuan, D. Y., He, W. G., Min, W., Ren, Z. K., Liu, X. W., et al. (2013). Geometric pattern and active tectonics in Southeastern Gansu province: Discussion on seismogenic mechanism of the Minxian-Zhangxian M_s 6.6 earthquake on July 22, 2013. *Chinese Journal of Geophysics*, 56(12), 4058–4071. <https://doi.org/10.6038/cjg20131211>. (in Chinese).

(Received September 20, 2018, revised January 19, 2019, accepted March 20, 2019, Published online April 4, 2019)